ELSEVIER

Journal of Nuclear Materials 307–311 (2002) 521–526

journal of nuclear materials

www.elsevier.com/locate/jnucmat

High resistance to helium embrittlement in reduced activation martensitic steels

A. Kimura [a,*], R. Kasada [a], K. Morishita [a], R. Sugano [a], A. Hasegawa [b], K. Abe [b], T. Yamamoto [c], H. Matsui [c], N. Yoshida [d], B.D. Wirth [e], T.D. Rubia [e]

[a] *Institute of Advanced Energy, Kyoto University, Gokasho Uji, Kyoto 611-0011, Japan*
[b] *Department of Engineering, Tohoku University, Aramaki, Aoba, Sendai 980-0845, Japan*
[c] *Institute for Materials Research, Tohoku University, Sendai 980-0812, Japan*
[d] *Research Institute for Applied Mechanics, Kyushu University, Fukuoka 816-0811, Japan*
[e] *Lawrence Livermore National Laboratory, Livermore, CA 94550, USA*

Abstract

Reduced activation martensitic steels (RAMSs) are the prime candidate structural material for the DEMO reactor and beyond where the material has been considered to suffer severe embrittlement caused by high-dose neutron irradiation and several thousands appm of transmutated helium. However, recent several works show high resistance to helium embrittlement of RAMS. Good performance of RAMS in the presence of rather high concentration of helium is considered to be due to high trapping capacity for helium atoms in the martensitic structure that consists of dislocations, lath boundaries, grain boundaries and carbide/matrix interfaces. To make clear the role of dislocations in trapping helium, thermal helium desorption spectra were measured for iron specimens annealed at different temperatures after cold work. A desorption peak, which increased its height with increasing dislocation density, was observed at around 550 °C, suggesting that dislocations trap helium atoms. A molecular dynamics simulation study for investigating the helium trapping behavior at helium–vacancy complexes suggests that helium is rather strongly bound to the complexes and increases the binding energy of vacancy to the complex, resulting in increasing stability of the complexes at elevated temperatures by reducing thermal emission of vacancies.

1. Introduction

Reduced activation 7–9Cr martensitic steels (RAMSs) have been the prime candidate for structural materials in the DEMO reactor and beyond [1–3], where the transmutation helium-induced embrittlement has been considered to be one of the critical issues for reactor operation [4,5]. There is a striking discrepancy in the interpretation of helium effects on RAMSs among research groups, where the discrepancy is well represented by the effects of helium on irradiation hardening and embrittlement. Especially, the role of helium–vacancy clusters or helium bubbles on irradiation hardening and cleavage fracture is thought to be a critical issue to be solved.

Previous isotope/tailoring experiments suggested a potential degradation effect of helium on RAMSs [6–11]. However, the authors investigated the effect of helium implantation on the ductile–brittle transition temperature by means of small punch (SP) test technique and concluded that an implantation with helium up to 580 appm below 432 K resulted in no enhancement of irradiation hardening and shift in the SP-DBTT to high temperature in a RAMS [12–14]. Since the concern of helium effects has influenced the strategy of RAFS R&D, the solution has been required towards applications to the ITER blanket test module and DEMO reactor.

* Corresponding author. Tel.: +81-774 38 3476; fax: +81-774 38 3483/3479.
E-mail address: kimura@iae.kyoto-u.ac.jp (A. Kimura).

0022-3115/02/$ - see front matter
PII: S0022-3115(02)01211-4

In this work, recent studies concerning helium effects on RAMSs are summarized and helium trapping mechanism is proposed to explain the highly resistant behavior of the steels against helium embrittlement.

2. Helium effects on RAMSs

2.1. Effects on high temperature properties

As shown in our previous work [15], neutron irradiation effects on the tensile properties strongly depend on irradiation temperature. Below 700 K, irradiation induces hardening, while it turns to softening above 700 K. At relatively high temperatures, helium can move and form He_mV_n complexes at defect sinks such as dislocations, lath boundaries and grain boundaries. Severe grain boundary embrittlement was often observed in austenitic steels implanted with several appm of helium [16–18]. In contrast to austenitic steels, ferritic steels are well known to be resistant to helium embrittlement at higher temperatures, as summarized in Table 1. Stamm and Schroeder [19] investigated the effects of post-implantation of helium up to 3040 appm on creep properties of a martensitic steel at 873 K and found no drastic effects on creep rupture time and fracture mode, although helium bubbles were observed after the tests. Lindau et al. [20,21] carried out fatigue tests by both in-beam and post-implantation methods, showing that fatigue life was reduced by 400 appm He at 693 K, while no effect of helium was observed at the helium concentration of 200 appm between 573 and 873 K, although helium bubbles were formed in the specimen. Hasegawa et al. [22] investigated the effects of 500 appm He on tensile properties above 673 K and showed that no significant effect was observed in the tensile strength and fracture mode. The high resistance to helium embrittlement of ferritic steels was attributed to the helium trapping mechanism. More recently, Yamamoto et al. [23] carried out creep tests for a reduced activation ferritic steel (F82H) implanted with helium up to 1000 appm at 823 K and observed no effects of helium on creep rupture time and fracture mode at 823 K.

From the experiments shown above, it is very likely that a few thousands appm helium never caused severe helium embrittlement above 673 K. It is considered that the high resistance of RAMSs against helium embrittlement is due to their martensitic structure, which contains a lot of trapping sites for helium and suppresses the aggregate of helium at grain boundaries.

At elevated temperatures, some helium can move to form helium bubbles at dislocations, lath boundaries and grain boundaries. Although the formation of helium bubbles was insufficient to induce embrittlement at elevated temperatures, there is a strong concern of low temperature embrittlement, namely a shift in DBTT,

Table 1
Summary of helium effects at elevated temperatures investigated by helium implantation method

Material	Range or thickness (mm)	Energy (MeV)	Temperature (K)	He concentration (appm)	dpa	Test method	He effects
DIN 1.4914 [19]	0.09	0–28	573–973	3040 (max)	–	Tensile and creep	No effect
Manet [21]	0.4	0–104	573–873	200	1.2	Fatigue at test temperature	No effect
Manet [20]	0.4	0–104	693	400	1.6	In situ fatigue	Reduction of lifetime
Ferritcs [22]	0.15	0–26	673, 773, 873	500	0.075	Tensile	No effect
F82H [23]	0.06–0.08	0–20	823	1000	–	Creep	No effect

caused by helium bubbles. The other concern is enhancement of irradiation hardening by helium, since the helium and helium–vacancy complexes trapped at dislocations might have a potential to cause enhancement of irradiation hardening or embrittlement at low temperatures.

2.2. Effects on DBTT shift

Many studies have been done to investigate helium effects on the irradiation-induced DBTT shift. The dependence of the DBTT shift on helium concentration is summarized in Fig. 1 where many discrepancies were observed among the data.

2.2.1. Boron-10 technique

Utilizing the nuclear transmutation reaction $^{10}B(n, \alpha)^{7}Li$, helium effects were often investigated for fusion structural materials. Since natural boron contains about 20% ^{10}B, helium was produced in the neutron-irradiated steels that contains natural boron as an alloy element. Effects of boron on the DBTT of several kinds of ferritic steels are summarized in Table 3 of Ref. [11,12], showing disagreement in the results among researchers. Rieth et al. [11] investigated effects of neutron irradiation on the DBTT of several kinds of ferritic steels, which contain different amounts of boron, and showed that the ΔDBTT of the steel increased with increasing boron concentration. They attributed the difference in the ΔDBTT to the difference in the amount of transmutation helium in the steels. It is, however, considered that the difference in the ΔDBTT is due to the difference in the steel in itself. The ΔDBTT should be compared among the same kind of steels. In order to detect helium effects on F82H, Shiba and Hishinuma [12] investigated the boron effect on the DBTT of F82H that contains either natural boron or boron-10. Since the ΔDBTT was larger in the steel containing boron-10, they concluded that the transmutation helium enhanced irradiation embrittlement of the steel. On the contrary, Yamamoto et al. [24] showed that there was no significant difference in the ΔDBTT between high purity steels doped with natural boron and boron-10, in which the transmutation helium is evaluated to be 14 and 65 appm, respectively, following neutron irradiation to 0.12 dpa at 563 K in the Japan Materials Test Reactor. The discrepancy between these two researchers can be explained in terms of the difference in the nitrogen concentration between the steels they used. The nitrogen concentration in F82H and high purity steel is 0.015 and <0.001 wt ppm, respectively. Since boron nitrides are rather thermally stable, many nitrogen atoms are in the form of boron nitrides before irradiation. After the transmutation, boron nitrides decompose into lithium and nitrogen atoms, which may have a potential of embrittlement of the steels. Although the boron-10 technique is convenient to produce helium in the materials, the following effects should be taken into account: (1) distribution of helium atoms, (2) disappearance of boron atoms, (3) production of lithium atoms, (4) helium/dpa ratio.

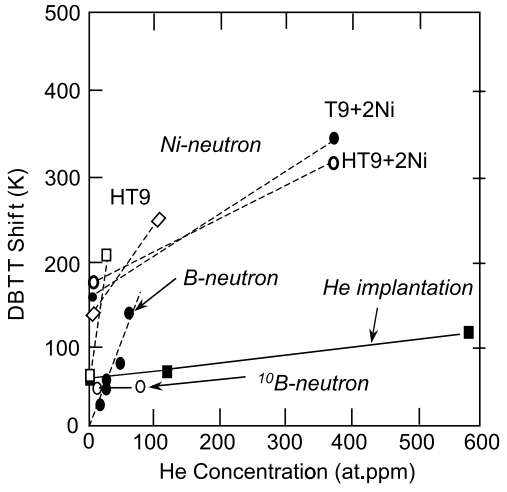

Fig. 1. Dependence of DBTT shift on helium concentration obtained by several researchers with different test techniques.

2.2.2. Ni addition technique

In this case, helium is produced by a two-step reaction, $^{58}Ni(n, \gamma)^{59}Ni$ (n, $\alpha)^{56}Fe$, and a relatively large amount of nickel (1–2 wt%) is added to the steels. Klueh et al. [6,7] measured the DBTT of the steels with and without addition of nickel and found larger ΔDBTTs in the steels added with nickel, which was interpreted in terms of helium-enhanced ductility loss. Gelles et al. [10] compared the bulge deformation behavior among the steels added with ^{58}Ni and ^{60}Ni, and both by means of the shear punch test method, and showing no significant difference in the deformation behavior among the steels. Since helium is not produced from ^{60}Ni, the change in the deformation behavior of the steel added with and without ^{60}Ni is attributed to the nickel addition itself. Kasada et al. [25] irradiated with neutrons to a RAMS with and without nickel addition at 550 K up to 2.2 dpa in the Advanced Test Reactor, and found that the steel added with 1 wt% nickel showed a two times larger irradiation hardening than the steel without nickel addition. Examinations by TEM revealed that the size and number density of dislocation loops were smaller and higher, respectively, in the steel added with nickel, indicating that large irradiation hardening observed in the nickel added steel is due to the increase in the number density of dislocation loops. It is expected that an iron–nickel dumbbell is more stable and easily to form smaller dislocation loops that induce the additional hardening. Helium effects on the fracture behavior can be extracted

by comparing fracture behavior between the steels with addition of ^{58}Ni and ^{60}Ni.

2.2.3. Helium implantation method

The effects of helium implantation on DBTT were investigated for a RAMS by means of the SP test technique [26,27]. Homogeneous implantation with 580 appm of helium below 423 K resulted in a hardening, $\Delta HV = 96$, and a shift in SP-DBTT by 39 K that corresponds to the shift in CVN-10-DBTT of 98 K estimated from an empirical equation, which were well interpreted in terms of displacement damage, and no enhancement of the DBTT shift and hardening by helium was observed. As for fracture mode at lower temperatures, no intergranular fracture was observed. Transmission electron microscopy revealed that no helium bubbles were formed in as-implanted specimens but many helium bubbles exist in the specimen after post-implantation annealing to 873 K.

A series of TEM observation studies during annealing revealed that helium bubble formation appears to occur at grain boundaries after annealing above 723 K [28]. This suggests that during implantation at low temperature (<423 K), helium atoms are captured at trapping sites, such as vacancies, vacancy clusters, dislocations and lath boundaries. This results in suppression of the aggregation of large amounts of helium to form helium bubbles in the matrix as well as at grain boundaries. To investigate the effect of helium bubbles on the fracture behavior, the specimen implanted with helium to 580 appm was fractured at 77 K in a bulge deformation mode after post-implantation annealing to 873 K. Of notice is that even in the existence of helium bubbles at grain boundaries, the fracture mode was a complete cleavage and no intergranular fracture was observed. Fig. 2 shows the recovery behavior of hardening and the interpretation of helium bubble formation in a RAMS during annealing after helium implantation at below 423 K.

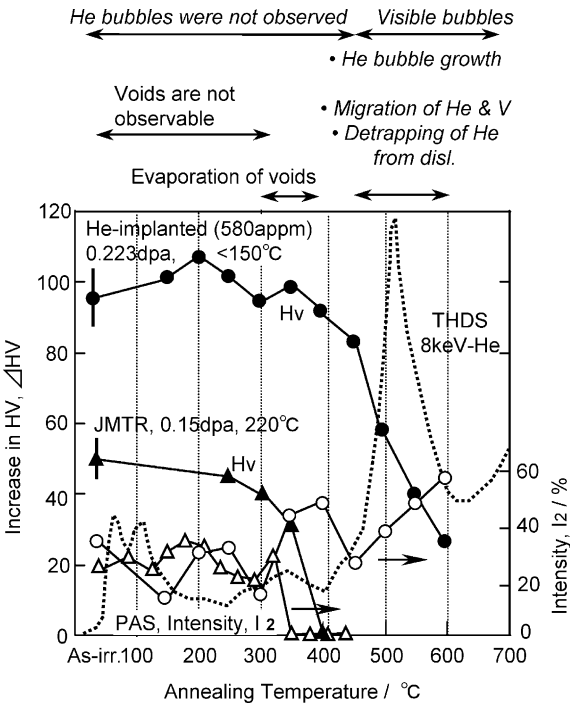

Fig. 2. Post-irradiation annealing behavior of Vickers hardness, positron lifetime and helium desorption. Elementary processes are also shown in the top of the figure.

3. Helium trapping behavior

3.1. Trapping capacity of helium in the martensitic structure

Trapping of helium in the martensitic structure causes a reduction of helium bubble formation at grain boundaries, resulting in suppression of grain boundary helium embrittlement. As for the effects of helium trapping in the matrix of RAMS on the deformation and fracture behavior, recent several studies also indicate no enhancement of both the irradiation hardening and embrittlement, as shown above. It is considered that helium trapping in the matrix also retards helium bubble growth to a large size in a high density enough to cause detrimental effects on mechanical properties.

The trapping capacity of helium in the martensitic structure of RAMSs was estimated with an assumption that each lattice site, which is involved in dislocations, lath boundaries, grain boundaries, interfaces of precipitate/matrix, serves as a trapping site for helium. Here, the trapping capacity increases with decreasing grain size and increasing dislocation density, and so on. Characteristic numbers shown in Table 2 were obtained by TEM observation of the martensitic structure in a RAMS. The ratio of the number of trap sites and the number of total lattice sites in a unit volume gives the concentration of trapping sites, and is shown in the fourth column. A simple estimation of trapping site concentration indicates that the trapping capacity of dislocations is much higher than that of grain boundaries: more than two orders of magnitude. It is also pointed out that the total concentration of the trapping sites is estimated to be about 2700 appm, and when a trapping site captures several helium atoms, the trapping capacity will increase more, as indicated in the last column. As for vacancy clusters, the trapping capacity may become large when the helium/vacancy ratio is higher than one. More important is that the nucleation sites of helium–vacancy complexes are involved be in the martensitic structure.

Table 2
An estimation of helium trapping capacity of martensitic structure in a RAMS

Structures	Characteristic numbers		Trap site ratio (ppm)	He/trap site
Grain boundaries	Grain size	33 μm	≈10	1–3
Lath boundaries	Lath size	2.8 μm	≈100	1–3
Dislocations	Density	$5 \times 10^{17}/m^2$	≈1700	1–3
Precipitates	Average size, density	60 nm, $2 \times 10^{20}/m^2$	≈500	1–3
V-clusters	Average size, density	2 nm, $3 \times 10^{21}/m^3$	300	1–6
Total	–	–	2910	2910–10 230 ppm

He/trap site ratios depend on the binding energy of helium to the cluster, namely, temperature.

3.2. Thermal helium desorption behavior

Helium trapping by dislocations was investigated [29] by means of thermal helium desorption measurements in pure iron implanted at room temperature with collimated, mass-analyzed beams of mono-energetic He^+ ions. The incident energies were 8 keV and 150 eV, respectively, by which atomic displacement damage does and does not take place in iron. Prior to helium implantations, the specimens were plastically deformed by rolling at room temperature, followed by annealing at 573, 873 and 1073 K for 2, 12 and 2 h, respectively. Vickers hardness and positron lifetime measurements were performed before implantation and the results were summarized in Table 3, indicating that the cold work almost fully recovered in the PR2 specimens but a part of cold work still remained in the PR1 specimen. According to the positron lifetime measurements, vacancies were also produced by the plastic deformation, but they are considered to anneal out after annealing above 673 K. Fig. 3 shows helium thermal desorption spectra of four types of pure iron. In the CW, PR1 and PR2 specimens, a clear desorption peak appeared at around 830 K. The plastic deformation-induced peak becomes small with recovery of dislocation by annealing. In other words, as the dislocation density decreased, the peak height gradually decreased. Therefore, this peak may correspond to desorption of helium atoms trapped by dislocations. Thermal helium desorption spectra were also obtained for a RAMS implanted with helium ions at room temperature, indicating the same peak in the temperature region. It is suggested that the dislocations

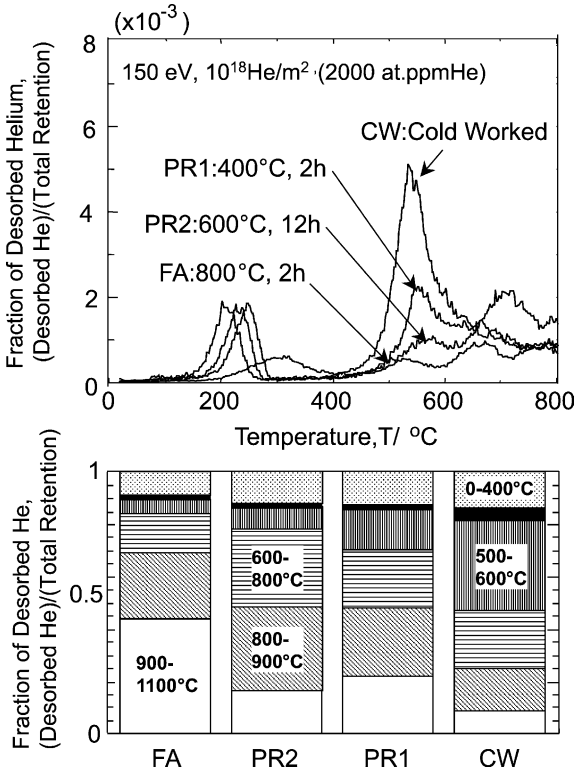

Fig. 3. THDS (top) and fraction of desorbed He at a temperature regime (bottom) in cold worked and annealed pure irons.

Table 3
Results of Vickers hardness and positron lifetime measurement of cold worked and annealed pure iron

	Vickers hardness	Positron lifetime (ps)
CW (cold worked)	180	148
PR1 (anneal: 673 K, 2 h)	110	–
PR-2 (anneal: 873 K, 12 h)	74	110
FA (anneal: 1073 K, 2 h)	62	110

efficiently trap helium and/or helium–vacancy complexes in martensitic steels, and retard the formation of helium bubbles in the matrix as well as at grain boundaries.

3.3. Molecular dynamics (MD) calculations

An MD calculation study was performed to investigate the formation energies of helium–vacancy complexes (He_nV_m; $n \geqslant 0$ and $m \leqslant 20$) in bcc iron [30]. The formation energy of an interstitial helium atom and a vacancy to a helium–vacancy complex was determined as a function of the numbers of helium atoms and vacancies in the complex. The binding of helium and

vacancy to a helium–vacancy complex greatly depends on the helium-to-vacancy ratio of the complex. When the ratio is close to zero, helium binding energy almost equals to the formation energy of interstitial helium in bcc iron (5.25 eV), and decrease with increasing the ratio. The binding energy of vacancies to a helium–vacancy complex shows an increasing and a decreasing function of the helium-to-vacancy ratios of the complex when the ratio is relatively lower and extremely higher, respectively. For the complex with relatively lower ratios, the vacancy binding energy ranges from about 1 eV at the ratio of zero to about 6.5 eV at the ratio of about 6 He/vacancy. This indicates that helium can stabilize the complex, thereby increasing the thermal stability of the complex by reducing the thermal emission of vacancies. The MD calculations suggest that helium is strongly bound to the helium–vacancy complexes and may play an important role on the microstructural evolution in RAMS during irradiation.

4. Summary

RAMSs are not highly susceptible to helium embrittlement at temperatures between RT and 873 K up to several hundreds appm of helium. Highly resistant properties of the steels against helium embrittlement are considered to be due to helium trapping effects in the martensitic structure that consists of dislocations, lath boundaries, carbides and precipitates in high density. An MD calculation study suggests that helium is strongly bound to helium–vacancy complexes. The helium trapping capacity of the martensitic structure in RAMS will be critical for the assessment of the feasibility of the steel as fusion structural material for the DEMO reactor and beyond.

References

[1] T. Morimura, A. Kimura, H. Matsui, J. Nucl. Mater. 239 (1996) 118.
[2] A. Kimura, M. Narui, T. Misawa, H. Matsui, A. Kohyama, J. Nucl. Mater. 258–263 (1998) 1340.
[3] A. Hishinuma, A. Kohyama, R.L. Klueh, D.S. Gelles, W. Dietz, K. Ehrlich, J. Nucl. Mater. 258–263 (1998) 193.
[4] H. Ullmaier, Nucl. Fusion 24 (8) (1984).
[5] H. Schroeder, J. Nucl. Mater. 155–157 (1988) 1032.
[6] R.L. Klueh, D.J. Alexander, J. Nucl. Mater. 179–181 (1991) 733.
[7] R.L. Klueh, P.J. Maziasz, J. Nucl. Mater. 187 (1992) 43.
[8] R. Kasada, A. Kimura, H. Matsui, M. Narui, J. Nucl. Mater. 258–263 (1998) 1199.
[9] R. Kasada, T. Morimura, H. Matsui, M. Narui, A. Kimura, ASTM STP 1366 (2000) 448.
[10] D.S. Gelles, G.L. Hankin, M.L. Hamilton, J. Nucl. Mater. 258–263 (1998) 1147.
[11] M. Rieth, B. Dafferner, H.D. Röhrig, J. Nucl. Mater. 258–263 (1998) 1147.
[12] K. Shiba, A. Hishinuma, J. Nucl. Mater. 283–287 (2000) 474.
[13] W.C. Leslie, The Physical Metallurgy of Steels, in: McGraw-Hill Series in Mater. Sci. & Eng., 1982, p. 269.
[14] R. Lindau, A. Möslang, D. Preininger, M. Rieth, H.D. Röhrig, J. Nucl. Mater. 271&272 (1999) 450.
[15] A. Kimura, T. Morimura, M. Narui, H. Matsui, J. Nucl. Mater. 233–237 (1996) 319.
[16] H. Schroeder, P.J. Batfalsky, J. Nucl. Mater. 117 (1983) 287.
[17] H. Trinkaus, J. Nucl. Mater. 133&134 (1985) 105.
[18] H. Schroeder, J. Nucl. Mater. 155–157 (1988) 1032.
[19] U. Stamm, H. Schroeder, J. Nucl. Mater. 155–157 (1988) 1059.
[20] R. Lindau, A. Möslang, J. Nucl. Mater. 212–215 (1994) 599.
[21] R. Lindau, A. Möslang, J. Nucl. Mater. 179–181 (1991) 753.
[22] A. Hasegawa, H. Shiraishi, H. Matsui, K. Abe, J. Nucl. Mater. 212–215 (1994) 720.
[23] N. Yamamoto et al., these Proceedings.
[24] T. Yamamoto et al., these Proceedings.
[25] R. Kasada et al., these Proceedings.
[26] A. Kimura, T. Morimura, R. Kasada, H. Matsui, A. Hasegawa, K. Abe, ASTM STP 1366 (2000) 626.
[27] R. Kasada, A. Kimura, A. Hasegawa, H. Matsui, J. Nucl. Mater. 299 (2001) 83.
[28] A. Kimura, R. Kasada, R. Sugano, A. Hasegawa, H. Matsui, J. Nucl. Mater. 283–287 (2000) 827.
[29] R. Sugano, K. Morishita, H. Iwakiri, N. Yoshida, A. Kimura, these Proceedings.
[30] K. Morishita, B.D. Wirth, T.D. Rubia, A. Kimura, in: The Proceedings of PRICM4, Japan Institute of Metals 2001.